Regular Article

PHYSICAL CHEMISTRY RESEARCH
Published by the
Iranian Chemical Society
www.physchemres.org
info@physchemres.org

***Phys. Chem. Res.**, Vol. 5, No. 3, 585-600, September 2017*
DOI: 10.22036/pcr.2017.72773.1346

The Application of Hybrid RSM/ANN Methodology of an Iron-based Catalyst Performance in Fischer-Tropsch Synthesis

A. Razmjooie, H. Atashi* and F. Shahraki

Department of Chemical Engineering, Faculty of Engineering, University of Sistan and Baluchestan, Zahedan, Iran

(Received 12 January 2017, Accepted 13 May 2017)

In this research, the performance and kinetics of an iron/manganese oxide catalyst in a fixed-bed reactor is studied through the Fischer-Tropsch synthesis. The ranges of the operating conditions are P: 1-12 barg, T: 513-553 K, H_2/CO ratio: 1-2 and GHSV: 4200-7000 $\left(\frac{cm^3\,(STP)/h}{g_{cat}}\right)$. The effects of the independent variables on the Fischer-Tropsch synthesis product are analyzed using a statistical model based on the experimental data. The response surface methodology and artificial neural network are used to model the experimental data for the carbon monoxide conversion (CO% conversion) and CO consumption rate. Some of the statistical parameters such as correlation coefficient and mean square error are calculated to demonstrate the capability and sensitivity analysis of methods. The obtained results from the statistical methods show a good agreement with the experimental data. It is shown that the results of artificial neural network are more accurate than those of the response surface methodology. Moreover, the optimal conditions are obtained from the maximum amount of CO% conversion at P = 8 barg, T = 559.5 K, H_2/CO = 2.5 and GHSV = 7325.2 $\left(\frac{cm^3\,(STP)/h}{g_{cat}}\right)$ while the maximum amount of consumption rate of CO happens at P = 8 bar, T = 568 K, H_2/CO = 2.5 and GHSV = 2800 $\left(\frac{cm^3\,(STP)/h}{g_{cat}}\right)$. Finally, the entire quadratic equations for all of the variables and optimal conditions for the responses are explained, respectively.

Keywords: Fischer-Tropsch synthesis, Catalytic kinetic modeling, Response surface, Artificial neural network, Optimization

INTRODUCTION

In recent years, decreasing the energy resources has made governments search and replace alternative sources for crude oil. Among these attempts, the process of transforming synthesis gas to hydrocarbon mixture compounds (C_nH_{2n+2}, C_nH_{2n}), called Fischer-Tropsch synthesis (FTS), provides a promising approach to moderate crude oil consumption in the world. Fischer-Tropsch synthesis is a catalytic process in which syngas (H_2+CO) is converted into a variety of valuable hydrocarbons. Fischer-Tropsch synthesis is one of the most important processes for production of clean and sulfur-free hydrocarbons [1-6]. FTS is the second technology for the hydrocarbon production [7]. Catalysts play essential roles in FTS. Generally, the catalysts used for FTS are mainly iron and cobalt. Iron is an active catalyst for water-gas-shift (WGS) reaction. The hydrocarbon formation and WGS reaction kinetics have been studied systematically [8-14]. Kinetic study of FTS reaction based on the detailed reaction mechanism via Langmuir-Hinshelwood-Hougen-Watson (LHHW) method is very significant for the development of catalyst and industrial applications [15]. Typically, iron-based catalysts contain small amounts of potassium to improve the carbonization and suppress methane formation [16-18] and/or other metal promoters such as manganese, calcium, zinc, copper and magnesium to boost catalyst activity and selectivity [17,19].

*Corresponding author. E-mail: H.Ateshy@hamoon.usb.ac.ir

Among the promoted iron-based catalysts, the Fe-Mn catalyst has some industrial record and reportedly has a higher olefin and middle distillation cut selectivity [19-21]. There are many factors for FTS product distribution, such as pressure, temperature, H_2/CO ratio, space velocity (GHSV), type of catalyst, *etc*. Therefore, it is necessary to use the design of experiments to reduce costs and time.

There are two methods classified to model and predict experimental data. The first method is response surface methodology (RSM) which is a statistical method for development and formulation of experiment design. RSM makes a polynomial mathematical model to describe the relationship between the process factors and response. Using this method, researchers can evaluate influence of independent variables on the model and also the interaction of different parameters on each other.

Second method is artificial neural network (ANN) which is a strong model to predict and optimize chemical processes. ANN is a mathematical model based on the experimental data [22]. There are a few authors who have studied application of RSM and ANN techniques to predict and optimize the operating parameters on FTS [23-25]. In this study, the RSM and ANN results were analyzed by statistical errors such as correlation coefficient (R^2) and mean square error (MSE).

EXPERIMENT

Catalyst Preparation

The catalyst were prepared by incipient wetness impregnation of Al_2O_3 with aqueous iron nitrate ($Fe(NO_3)_2.6H_2O$) (0.5M) (99%, Merck) and manganese nitrate ($Mn(NO_3)_2.6H_2O$) (0.5M) (99%, Merck) solutions. First, the Al_2O_3 support was calcined before impregnation at 600 °C in flowing air for 6 h. For 50%Fe/50%Mn/5Mn/5wt.%Al_2O_3 catalyst, the iron and manganese nitrate solution dispersed through a spray needle into the support. The support dried at 120 °C C for 16 h and calcined at 550 °C for 6 h. The best surface area for the fresh catalyst was 120.2 (m^2 g^{-1}). The phases identified in the fresh catalyst included monoclinic Fe_2O_3, cubic MnO_2 and Mn_2O_3, orthorhombic $AlFeO_3$ orthorhombic and tetragonal Al_2O_3. The sample after the FT reaction, contained monoclinic Fe_2C, orthorhombic Mn_2O_3, orthorhombic Fe_3C, $FeFe_2O_4$, $MnAl_2O_4$/MnO and cubic Al_2O_3. One gram of fresh, 0.15-0.25 mm (60-100 ASTM mesh) catalyst reached with the simulated syngas, diluted 1 part to four with quartz of the same size.

Kinetic Studies

A differential fixed-bed micro reactor (ID = 6 mm, Length = 40 mm) provided steady state kinetic data, the detailed description is found elsewhere [26-28]. The heat transfer analysis indicated an essentially isothermal catalyst under these operating conditions, with predicted conversion results based on an isothermal, pseudo-homogeneous, one-dimensional and plug-flow model [28-30]. The schematic of experimental setup is shown in Fig. 1.

The model of equation consisting of a mass balance for each component is written as follows:

$$\frac{d(uC_n)}{dZ} + r_n\rho_\beta = 0 \tag{1}$$

where C_n is the concentration of component n (mol m^{-3}), u refers to the superficial velocity (m/s), r_n is the overall reaction rate of component n (mol/((kgcat.s)), and ρ_β is the catalyst bed density (kgcat/m^3). The overall synthesis reaction with the boundary conditions $C_n = C^0_n$ at reactor entrance (z = 0) can be written as follows:

$$iCO + \left(i + \frac{j}{2}\right)H_2 \rightarrow C_iH_j + iH_2O \tag{2}$$

where i is the average carbon chain length of the hydrocarbon product, and j is the average number of hydrogen atoms per hydrocarbon molecules. The operating conditions for tests were set in the following ranges: temperature = 513-553 (K), pressure = 1-12 (bar), GHSV = 4200-7000 $\left(\frac{cm^3\,(STP)/h}{g_{cat}}\right)$, and H_2/CO feed molar ratio = 1-2. An equimolar atmospheric pressure, 60 (ml min^{-1}) flow of H_2 and N_2 reduced the fresh catalyst in situ for 16 h at 300 °C. Then, the catalyst cooled to 180 °C, and flushed with N_2. An oxygen balance determined the amount of water, because the TCD-GC could not analyze water accurately. These ideal tubular reactors have the following characteristics [30]

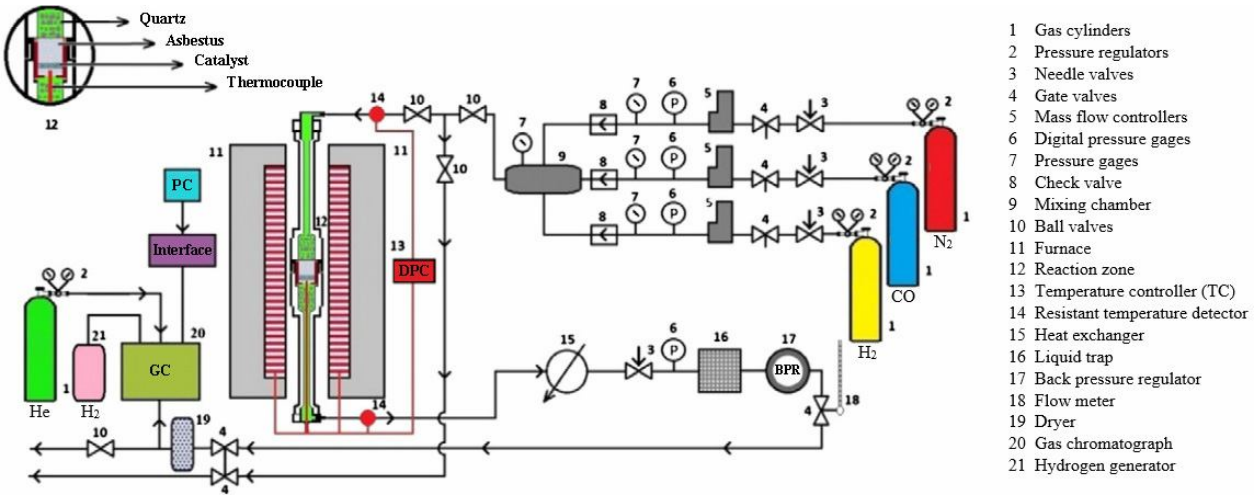

Fig. 1. Schematic diagram of the experimental setup [31].

$$\frac{ID}{D_P} \rangle 25 \tag{3}$$

To minimize by-pass:

$$\frac{H_b}{D_P} \rangle 100 \tag{4}$$

satisfying both relations minimized back-mixing. The carbon-containing products, determine CO conversion as follows:

$$X_{CO,out}(\%) = \frac{\sum n_i M_i}{M_{CO}} \tag{5}$$

where n_i is the number of carbon atoms in product i, M_i is the percentage of product i, and M_{co} is the percentage of CO in feed stream. The average of reaction rate is as follows:

$$-r_A = \frac{F_{CO}^0 X_{CO,out}}{W} \tag{6}$$

Kinetic Model Evaluation

The rate of syngas conversion depends on the partial pressure of the feed constituents, as well as temperature. In a reactor with the iron-based catalyst, CO absorbs more than H_2 at temperature above 77 °C [32]. Iron-based FT synthesis produces both water and carbon dioxide, representing two important routes for oxygen removal. While CO_2 has less effect on iron-based FT catalysts, water substantially affects intrinsic FT reaction rates [33,34]. Investigation evidence indicates that CO and water competitively absorbs on active sites of iron-based catalysts [35].

Response Surface Methodology

Response surface methodology (RSM) is a good statistical and mathematical technique for developing, improving and optimizing processes. The most extensive applications of RSM are particularly in situations where several input variables potentially influence some performance measure or quality characteristic of the product or process which is called response [36].

In this work, the effect of 4 important reactor conditions, pressure, temperature, H_2/CO ratio, and space velocity (GHSV), on CO conversion and consumption rate of CO have been studied *via* RSM. Finally, the results show a good agreement between experimental data and predicted model. The correlation between inputs and desired response could be represented as follows:

$$y = f(x_1, x_2, x_3, \ldots x_n) \pm \varepsilon \tag{7}$$

where y is the response, f is the function of response, $x_1, x_2, x_3, \ldots x_n$ are the inputs variables and ε is the fitting error.

A second order regression model was employed to fit the collection of experimental data, in this study. This model can be written as follows:

$$f = a_0 + \sum_{i=1}^{n} a_i x_i + \sum_{i=1}^{n} a_{ii} x_i^2 + \sum_{i<j}^{n} a_{ij} x_i x_j \pm \varepsilon \quad (8)$$

The model regression accuracy can be evaluated by a coefficient obtained from the following equation:

$$R^2 = 1 - \frac{SS_{res}}{SS_{tot}} \quad (9)$$

Adjusted R^2 is a modification of R^2that adjusts the number of explanatory terms in model. Adjusted R^2 is defined as following:

$$R^2_{adj} = 1 - \frac{MS_{res}}{MS_{tot}} \quad (10)$$

Artificial Neural Network

Artificial neural network (ANN) is a powerful mathematical method to solve nonlinear and complex problems in the science applications. The back propagation (BP) network technique with Levenberg-Marquadt Algorithm (LMA) was applied, in which the gradient descent method minimized the sum of square of network errors [37,38]. An ANN network usually consists of three layers: input layer, output layer and intermediate or hidden layer and was trained in three steps: feed forward of the input training pattern, back propagation of the related error, and the weights alteration [39,40]. Generally, a neuron can be determined by the following equation:

$$Y_i = \sum_{i=1}^{n} x_i \omega_i + \theta_i \quad (11)$$

where Y_i is the net input to the nod i in hidden or output layer, ω_i is the weight of component i, θ_i is bias and x_i is the input parameter as i. There are many factors to design a good ANN, such as the number of neurons in hidden layer, transfer function selection, training function algorithm and the number of input variables.

RESULT AND DISCUSSION

The effect of four input variables on CO conversion and consumption rate or CO ($-r_{co}$) reaction was performed based on central composite design (CCD). These variables are pressure, temperature, H_2/CO ratio and space velocity (GHSV). Table ***1*** shows the prediction capability of RSM, and ANN models compared to the experimental data for (CO% conversion).

Table ***2*** shows the prediction capability of RSM, and ANN models compared to the experimental data for ($-r_{co}$). The normal probability plot of residual was used to verify the model. If plot is normally distributed, then all points in this plot generally form a straight line. Fig. 2 shows which of two residual plots of responses were normally distributed.

The analysis of variance (ANOVA) was employed to evaluate the significance of model parameters, and insignificant ones were eliminated considering p-values. The fitness of model was determined by ANOVA. Tables 3, and 4 show the T-value and corresponding P-values, along with estimation coefficients for two responses. Lack-of-fit tests assess the fit of model. RSM automatically performs the pure error lack of fit test when data contain replicates (multiple, observation with identical x-values). The P-value is the probability of obtaining a statistical test that is at least as extreme as the calculated value is the null hypothesis is true.

The lesser values for P-value and the larger values for T-value indicated that the corresponding variables would be more significant. The response surface plots for (CO% conversion) are shown in Fig. 3. The full quadratic relating equations for (CO% conversion) with the four independent variables, namely pressure (x_1), temperature (x_2), H_2/CO ratio (x_3) and GHSV (x_4), are as follows:

$$\text{Yield (CO\% conversion)} = 0.246x_1 + 3.385x_2 - 6.91x_3 + 0.0043x_4 + 0.0012x_3x_4 - 0.003x^2_2 - 0.000001x^2_4 - 945 \quad (12)$$

Fig. 5 shows the influence of the four variables on the response ($-r_{co}$). Generally, pressure and temperature had positive effect on the response, also ($-r_{co}$) increased when

Table 1. Kinetic, ANN and RSM Results for Fe-MN/Al_2O_3 Catalyst in Fixed-bed Reactor for (CO% Conversion)

Run no.	P (x_1)	T (x_2)	H_2/CO (x_3)	GHSV(x_4)	Experimental	ANN	RSM
1	12	523	1	4200	7.44	7.353	8.52
2	4	523	2	4200	4.3	4.682	5.12
3	8	523	2	4200	6.83	6.801	5.24
4	1	523	2	4200	5.19	4.952	5.91
5	1	523	1.5	4200	5.86	6.225	6.17
6	12	523	1.5	4200	8.29	8.353	9.08
7	8	533	2	5000	7.67	7.758	8.45
8	1	533	2	5000	7.75	7.227	6.54
9	1	523	1.5	5000	7.09	6.524	8.13
10	8	533	1.5	5000	8.28	8.450	9.56
11	12	533	1.5	5000	9.11	9.034	8.16
12	1	533	1.5	5000	7.78	8.123	9.14
13	1	543	1	5000	10.19	10.45	12.1
14	8	513	1	5000	3.16	3.853	3.51
15	8	513	1.5	5000	4.03	4.967	4.70
16	4	513	1.5	5000	4.66	4.212	3.85
17	12	513	1	6000	5.29	5.832	4.82
18	1	513	1	6000	1.29	1.651	1.51
19	1	513	2	6000	3.36	3.125	2.36
20	8	513	1.5	6000	5.41	4.873	5.95
21	4	543	1	6000	9.73	9.126	10.87
22	8	543	1	6000	11.16	12.10	12.8
23	8	543	1.5	6000	12.25	12.89	13.7
24	1	533	1	7000	5.46	5.052	4.11
25	8	533	1	7000	9.23	9.952	10.56
26	4	533	1	7000	6.75	6.215	7.32
27	4	543	1	7000	8.21	7.347	7.82
28	1	543	1	7000	7.28	7.372	7.66
29	1	543	1.5	7000	8.53	8.661	9.15
30	4	543	1.5	7000	8.46	8.890	8.23

Table 2. Kinetic, ANN and RSM Results for Fe-MN/Al_2O_3 Catalyst in Fixed-bed Reactor for ($-r_{CO} \times 10^5$/mol mol^{-1} g^{-1})

Run no.	P (x_1)	T (x_2)	H_2/CO (x_3)	GHSV (x_4)	Experimental	ANN	RSM
1	12	523	1	4200	25.38	25.582	26.13
2	4	523	2	4200	25.21	25.681	26.12
3	8	523	2	4200	29.56	28.902	28.03
4	1	523	2	4200	21.25	21.810	22.41
5	1	523	1.5	4200	14.79	15.151	13.51
6	12	523	1.5	4200	31.18	31.472	32.82
7	8	533	2	5000	28.49	28.951	30.12
8	1	533	2	5000	22.71	22.266	21.37
9	1	523	1.5	5000	11.42	11.912	12.56
10	8	533	1.5	5000	17.04	17.012	17.45
11	12	533	1.5	5000	29.24	29.212	28.92
12	1	533	1.5	5000	16.47	16.911	17.85
13	1	543	1	5000	21.56	22.451	21.12
14	8	513	1	5000	15.39	14.930	15.02
15	8	513	1.5	5000	12.72	12.301	11.12
16	4	513	1.5	5000	15.13	15.591	16.78
17	12	513	1	6000	16.61	16.032	16.21
18	1	513	1	6000	11.35	11.031	11.92
19	1	513	2	6000	13.55	14.122	14.88
20	8	513	1.5	6000	15.16	15.810	14.12
21	4	543	1	6000	17.72	18.110	16.12
22	8	543	1	6000	3.41	3.5012	4.11
23	8	543	1.5	6000	22.74	22.211	22.12
24	1	533	1	7000	11.64	11.901	10.12
25	8	533	1	7000	3.68	3.551	4.754
26	4	533	1	7000	11.91	11.252	10.12
27	4	543	1	7000	14.77	14.121	15.76
28	1	543	1	7000	13.26	13.781	12.11
29	1	543	1.5	7000	12.53	12.340	14.12
30	4	543	1.5	7000	14.1	14.543	14.54

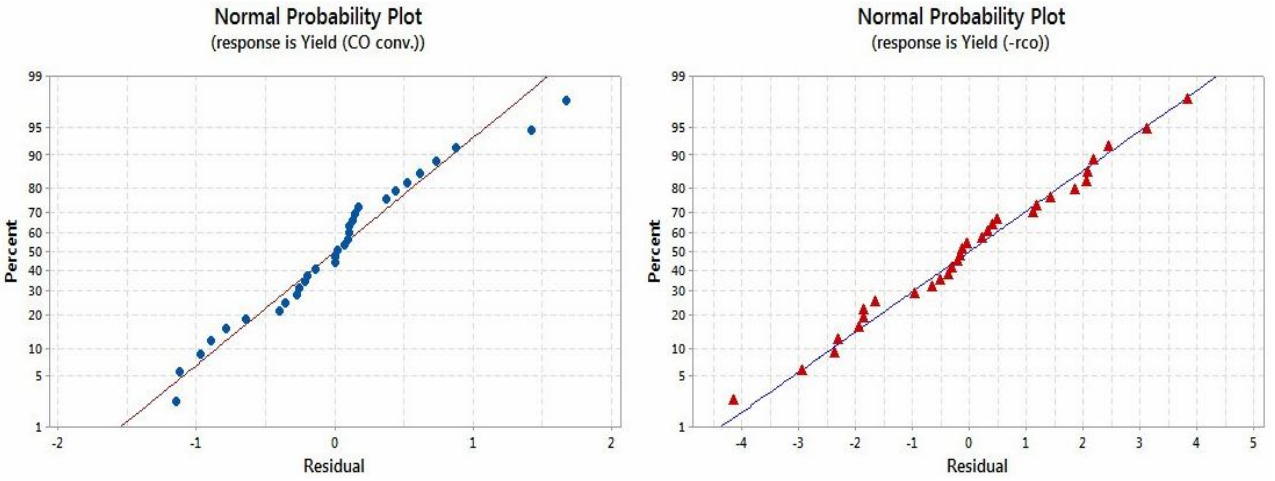

Fig. 2. Normal probability plots of two responses.

Table 3. Analysis of Variance (ANOVA) of the RSM Modeling for (CO% Conversion)

`	SE coefficient	T-value	P-value
Constant	0.209	48.36	0.000
Pressure	0.154	3.20	0.004
Temperature	0.154	12.52	0.000
H_2/CO	0.154	0.42	0.677
GHSV	0.154	4.66	0.000
Temperature*Temperature	0.140	-4.87	0.000
GHSV*GHSV	0.140	-7.12	0.000
H_2/CO*GHSV	0.189	4.66	0.000
Lack-of-fit			0.218
R-sq			98.40%
R-sq (adj)			96.08%

H_2/CO ratio rose. The full quadratic relating equation for ($-r_{co}$) is as follows:

$$\text{Yield } (-r_{CO}) = -0.528x_1 + 0.554x_2 + 4.86x_3 + 0.0294x_4 + 1.029x_1x_3 - 0.000056x_2x_4 + x_3x_4 + 3.7x^2_3 - 277.5 \quad (13)$$

In optimization part, Fig. 5 shows the effect of independent variables on two responses. Table 4 shows the RSM maximization of (CO% conv.) and ($-r_{co}$) with the best conditions of (P (bar), T (K), H_2/CO and GHSV $\left(\frac{cm^3\,(STP)/h}{g_{cat}}\right)$:

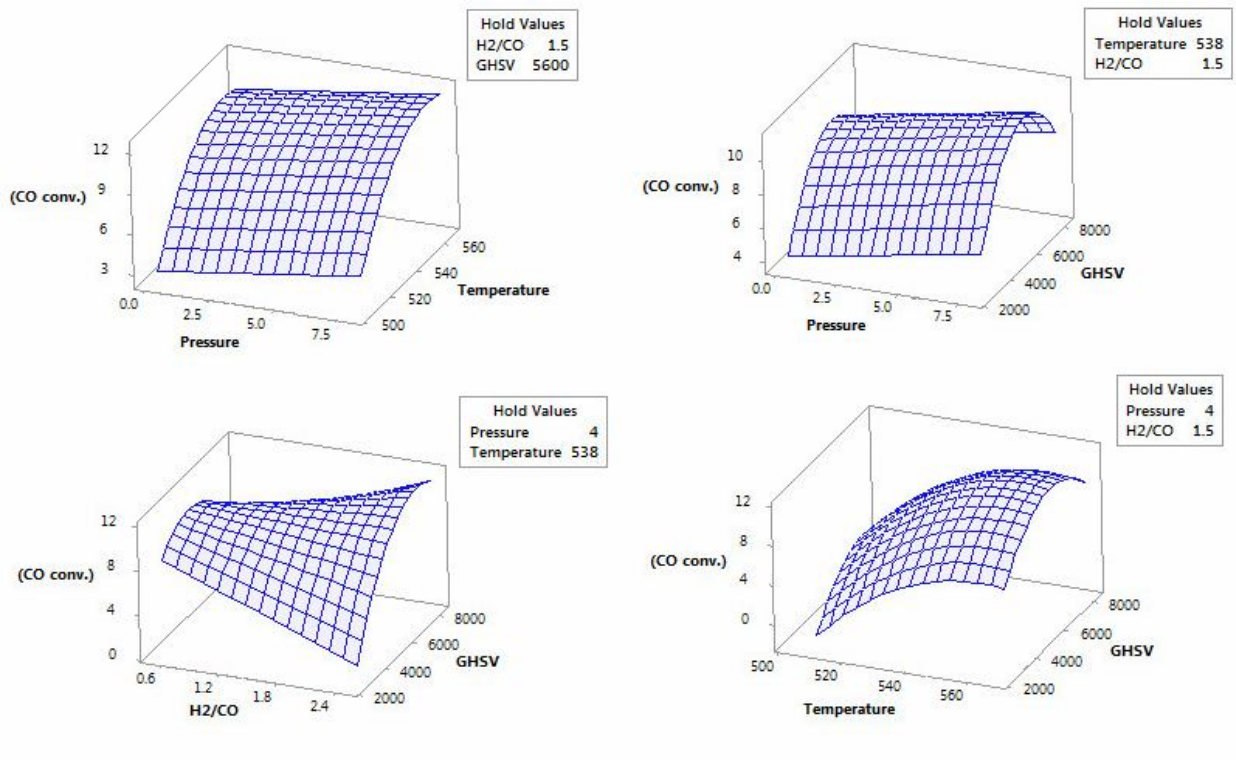

Fig. 3. Surface plots for the effect of four variables on the response (CO% conversion).

Table 5. Analysis of Variance (ANOVA) of the RSM Modeling for ($-r_{co}$)

Terms	SE coefficient	T-value	P-value
Constant	0.501	37.88	0.000
Pressure	0.446	4.56	0.000
Temperature	0.446	8.07	0.000
H_2/CO	0.446	9.80	0.000
GHSV	0.446	-11.90	0.000
H_2/CO*H_2/CO	0.403	2.30	0.032
Pressure*H_2/CO	0.546	1.89	0.073
Temperature*GHSV	0.546	-2.16	0.042
H_2/CO*GHSV	0.546	-2.59	0.017
Lack-of-fit			0.304
R-sq			97.89%
R-sq (adj)			95.40%

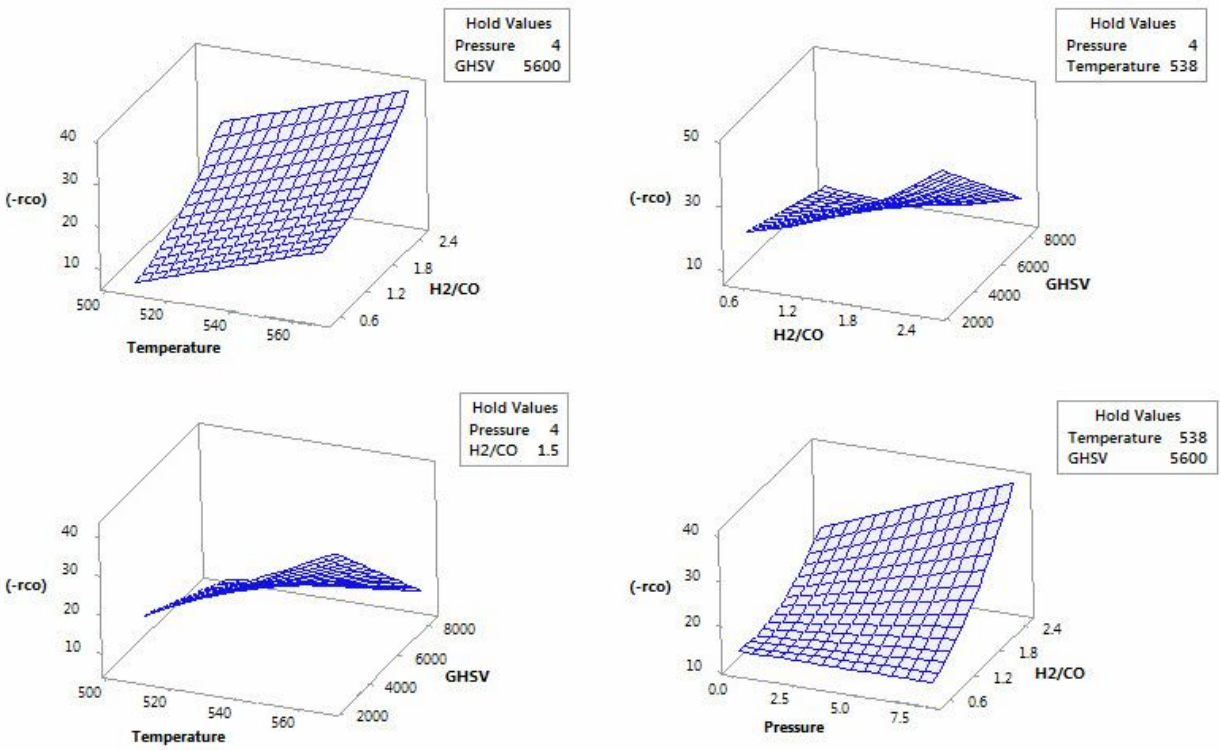

Fig. 5. Surface plots for the effect of four variables on the response ($-r_{co}$).

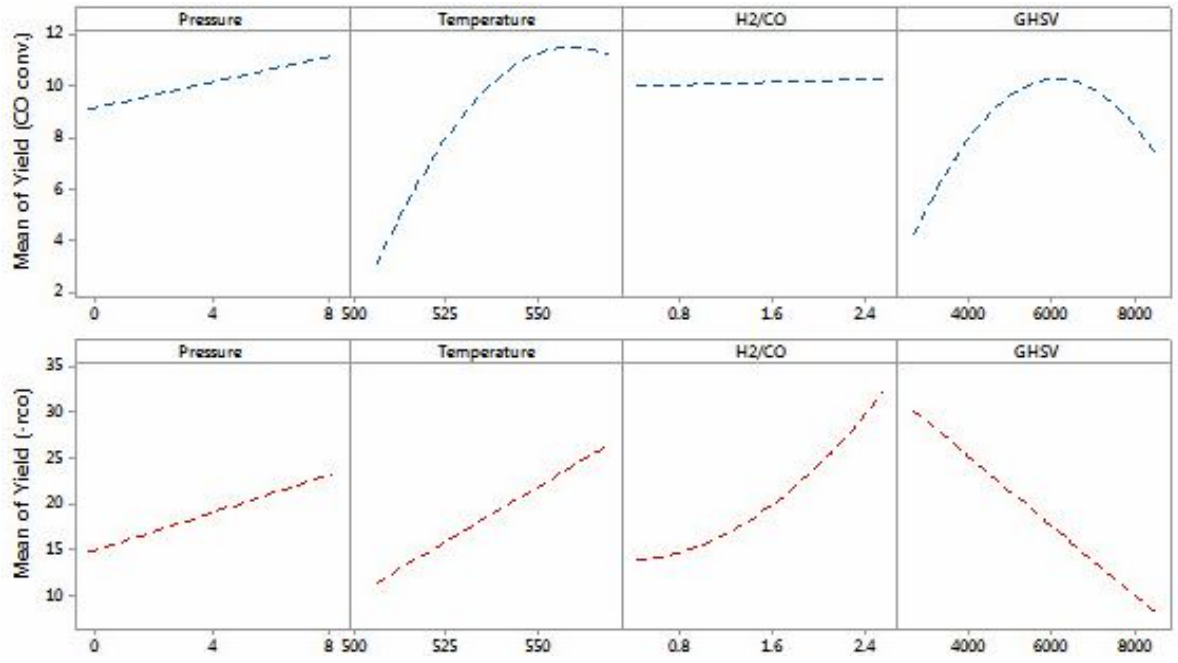

Fig. 5. Optimization plots of two responses.

Table 7. Maximization of Two Responses with Four Objectives

Term	P	T	H_2/CO	GHSV	Response
Max. of CO% conv.	8	559.5	2.5	7325.2	14.1
Max. of $-r_{co}$	8	568	2.5	2800	67.7

Table 7. Determined Specifications for the Best ANN Model

Algorithm	Feed-forward back propagation
Training Function	Levenberg-Marquardt (trainLM)
Hidden layer transfer function	Tangent sigmoid (tansig)
Output layer transfer function	Pure line (purelin)
Number of input layer neuron	4
Number of hidden layer neuron	6
Number of output layer neuron	1

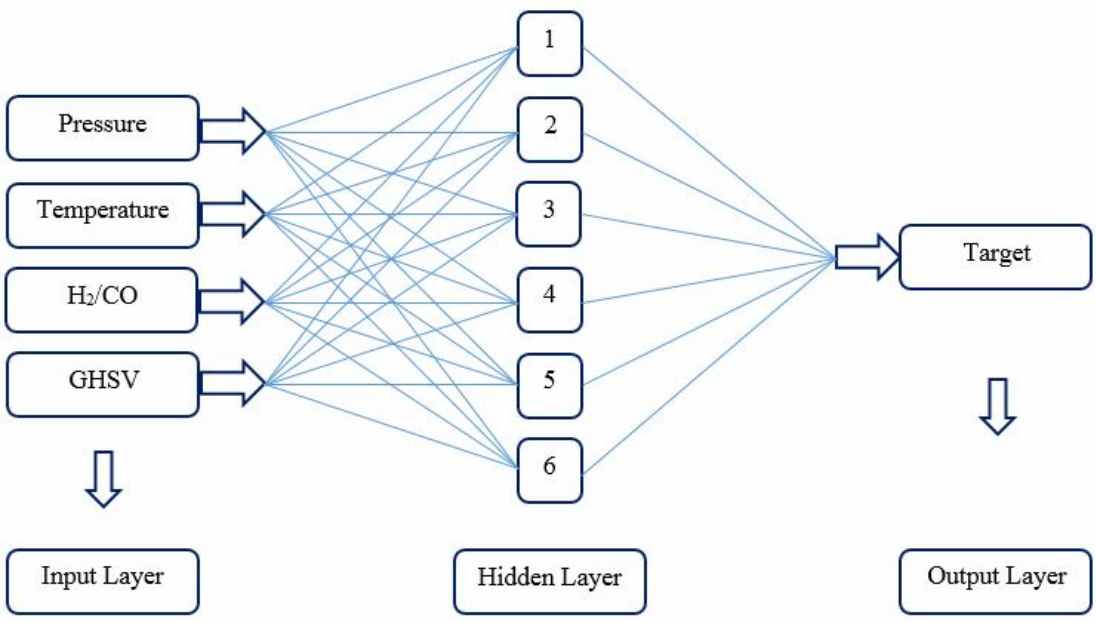

Fig. 6. Schematic diagram of the ANN model with input, hidden and output layers.

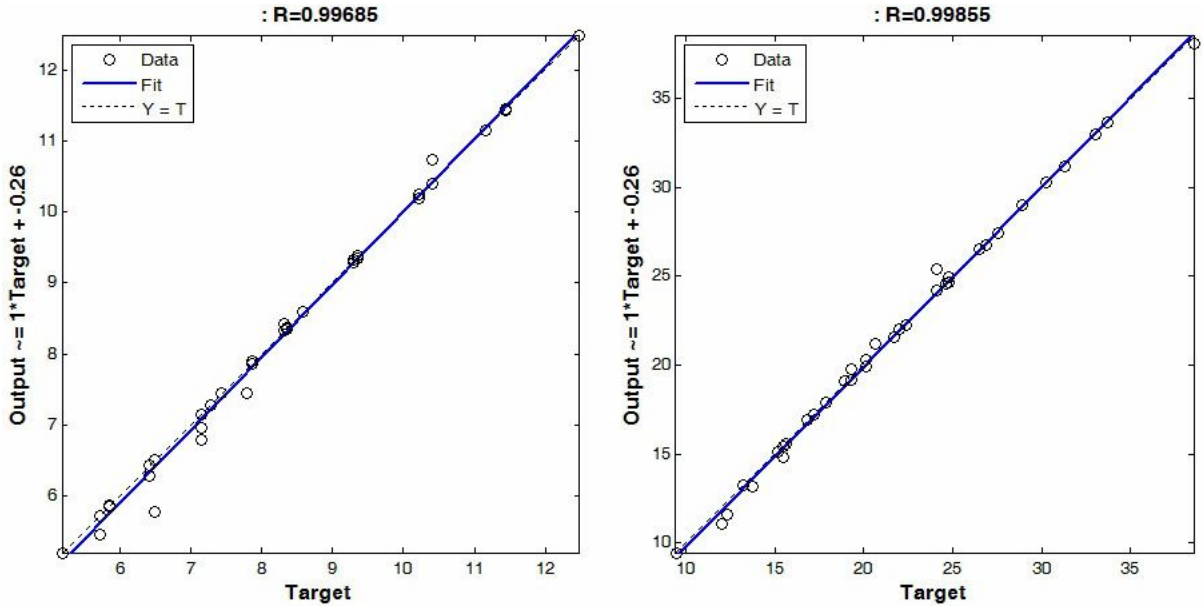

Fig. 8. The plots of experimental data *vs*. ANN model for %CO conv. (left) and -r_{co} (right).

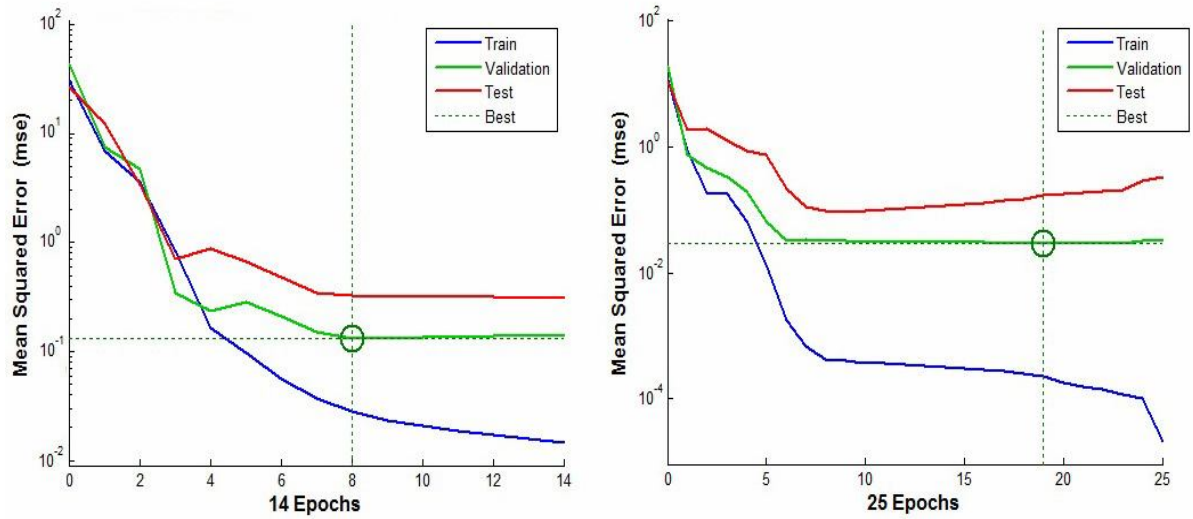

Fig. 8. MSE values of the developed ANN design at different epochs for the best network (best performance for (%CO conv.) are 0.0285 at epoch 25 and for (-r_{co}) is 0.1380 at epoch 14).

Comparison between RSM and ANN Models

This step presents the comparison between the predictive capability of RSM and ANN for two data sets, the experimental data used for developing the models (CO% conversion) and (-r_{co}). ANN modeling is determined based on four steps: 1. Preparation of the input values, 2. Suitable back propagation algorithm selection, 3. Selection of a suitable number of hidden layers, 4. Training and validation of model. Fig. 6 shows the ANN model layers. Four variables were used as the input variables (P, T, H_2/CO and GHSV), with 6 neurons as hidden layers. There are many types of training algorithm, and it is very difficult to understand which of them is efficient for ANN [2,41].

The Levenberg-Marquardt back propagation algorithm

Table 8. All of ANN Model Performances for (CO% Conversion) and ($-r_{co}$)

Performance	CO% Conversion	$-r_{co}$
MSE (performance)	0.0285	0.1380
Train performance	2.2498e-04	0.0082
Validation performance	0.0292	0.5454
Test performance	0.1750	0.4054

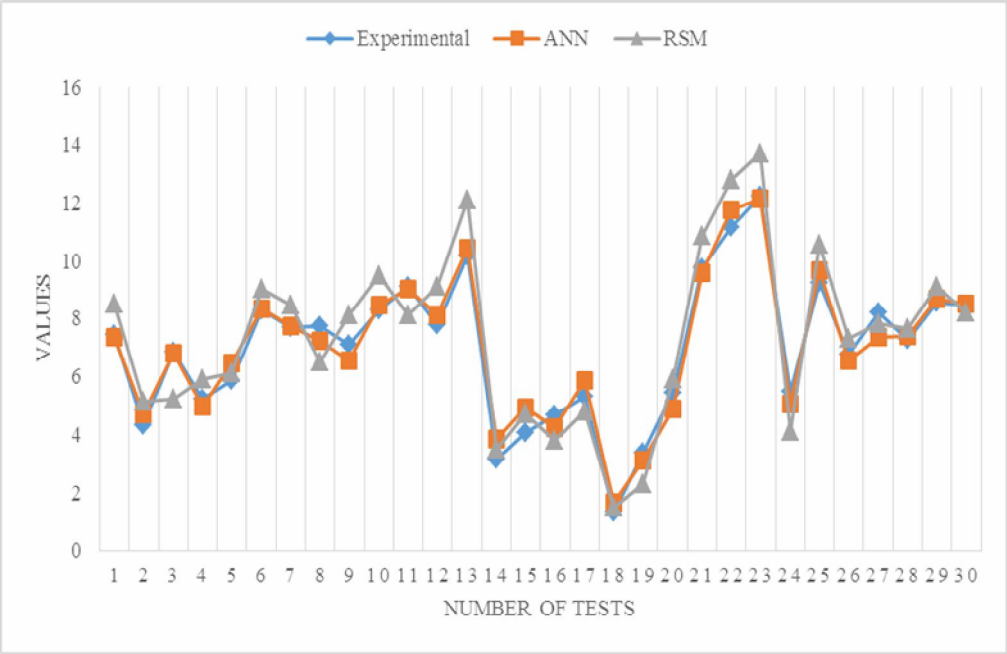

Fig. 9. Comparison between the experimental, ANN and predicted RSM for (CO% conversion).

(LMP) was used to ANN design. This algorithm was the best choice for this work, because it was trains fast and uses a tansigmoid transfer function (tansig) for hidden layer, and linear transfer function (purline) for output layer [39]. The ANN specifications are shown in Table 9.

ANN diagrams are shown in Fig. 8 (for both of (CO% conversion) and ($-r_{co}$) experimental data). These plots show the general adaptation between the experimental and predicted model data. To evaluate and verify the accuracy of models, two statistical values namely, mean square error (MSE) and ANN performances, are defined as the following:

$$MSE = \frac{1}{n}\sum_{i=1}^{n}(Y^{i,model} - Y^{i,exp})^2 \quad (14)$$

where $Y^{i,mod}$, $Y^{i,exp}$, $\overline{Y}$ and n are predicted model response, the experimental data, the mean value of the experimental data and the number of experimental data, respectively. Fig. 8 shows the variation of the MSE values for testing, validation and training of the developed ANN for two models. The best validation performance (MSE) for (CO conv.) is 0.0285 at epoch 25, and 0.1380 at epoch 14 for ($-r_{co}$).

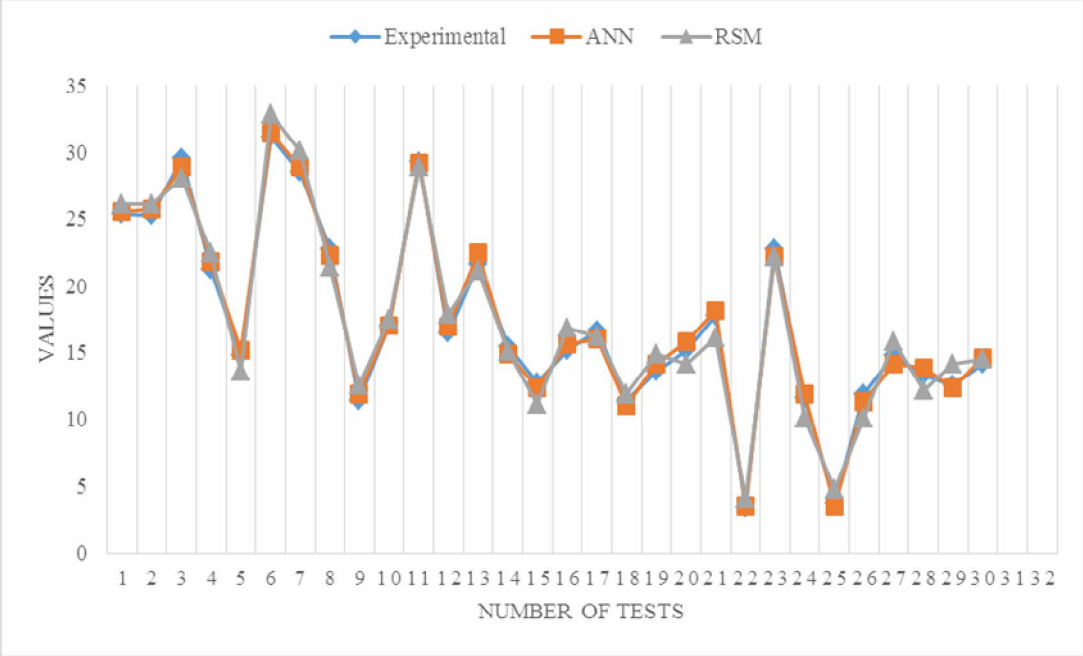

Fig. 10. Comparison between the experimental, ANN and predicted RSM for ($-r_{co}$).

Figures 9 and 10 that both models (ANN and RSM) have the ability to predict the experimental data for both studies. However, the predictive capability of ANN model is higher than that of the RSM model. This can be shown by evaluating the R^2 and MSE for both models (ANN, RSM).

CONCLUSIONS

In this study, the catalyst sample was prepared, and the conversion and kinetic reaction of CO over the well characterized catalyst was investigated. The RSM-CCD with four independent variables, pressure, temperature, H_2/CO ratio and space velocity (GHSV), and ANN with six neurons in hidden layers were used to make pattern to predict the experimental data. Also, the effect of four independent variables on (CO% conversion) and ($-r_{co}$) have been studied by RSM. The conversion of carbon dioxide growth was appreciably when pressure increased. At low GHSV, increase in H_2/CO ratio led to the response reduction, but a reverse trend was observed at high GHSV. CO% conversion increased with increasing the temperature and H_2/CO ratio, but at high temperature, this behavior was reverse. Also, consumption rate of carbon dioxide increased when H_2/CO ratio elevated. The consumption rate of CO increased appreciably when temperature rose. At low H_2/CO ratio, the effect of pressure increasing on response was negligible, but in high amount of H_2/CO led to rise in response. Furthermore, the consumption rate of CO collapsed when GHSV rose. These results indicated that the experimental data were so close to the estimated and predicted values by two methods, and demonstrated that the ANN model has a superior accuracy versus the RSM model. On the basis of the results, the maximum amount of responses were as follows: for CO% conversion was in P = 8 bar, T = 559.5 K, H_2/CO = 2.5, and for consumption rate of CO was in P = 8 bar, T = 568 K, H_2/CO = 2.5. Finally, these findings showed a high ability of the both models (ANN, RSM) to predict the experimental data.

ACKNOWLEDGEMENTS

The authors would like to gratefully acknowledge the University of Sistan and Baluchestan for their kindness and support in this research.

NOMENCLATURE

C_n	Concentration of component n (mol m^{-3})
u	Superficial velocity (m/s)
r_n	Overall reaction rate of component n (mol/((kgcat.s)))
ρ_β	Catalyst bed density (kgcat/m^3)
i	Average carbon chain length of the hydrocarbon product
j	Average number of hydrogen atoms per hydrocarbon molecules
n_i	Number of carbon atoms in product i
M_i	Percentage of product i
M_{co}	Percentage of CO in feed stream
F_{co}	Input flow rate of CO (mol s^{-1})
W	The weight of catalyst (kg)
X_{co}	CO conversion percentage
f	Function of response
$x_1, x_2, x_3, \ldots x_n$	RSM inputs variables
ε	Fitting error
SS_{res}	Residual sum of squares
SS_{tot}	Total sum of squares
MS_{res}	Residual mean of squares
MS_{tot}	Total mean of squares
Y_i	The net input to the nod i in hidden or output layer
ω_i	Weight of component i
θ_i	Bias index
x_i	Input parameter as i
n	Number of experiments
$Y^{i,mod}$	Predicted model response
$Y^{i,exp}$	Experimental data

REFERENCES

[1] Fu, T.; Lv, J.; Li, Z., Effect of carbon porosity and cobalt particle size on the catalytic performance of carbon supported cobalt Fischer-Tropsch catalysts. *Ind. Eng. Chem. Res.,* **2014**. *53*, 1342-1350, DOI: 10.1021/ie402128y.

[2] Adib, H.; Haghbakhsh, R.; Saidi, M.; Takassi, M. A.; Sharifi, F.; Koolivand, M.; Rahimpour, M. R.; Keshtkari, S., Modeling and optimization of Fischer-Tropsch synthesis in the presence of Co(III)/Al_2O_3 catalyst using artificial neural networks and genetic algorithm. *J. Nat. Gas Sci. Eng.,* **2013**. *10*, 14-24, DOI: 10.1016/j.jngse.2012.09.001.

[3] Bayat, M.; Hamidi, M.; Dehghani, Z.; Rahimpour, M.; Shariati, A., Sorption-enhanced reaction process in Fischer-Tropsch synthesis for production of gasoline and hydrogen: mathematical modeling. *J. Nat. Gas Sci. Eng.,* **2013**. 14, 225-237, DOI: 10.1016/ j.jngse.2013.06.011.

[4] Chiang, S. -W.; Chang, C. -C.; Shie, J. -L.; Chang, C. -Y.; Ji, D. -R.; Tseng, J. -Y., Synthesis of alcohols and alkanes over potassium and vanadium promoted molybdenum carbides. *J. Taiwan Inst. Chem. Eng.,* **2012**. *43*, 918-925, DOI: 10.1016/j.jtice.2012.07.008.

[5] Hemmati, M. R.; Kazemeini, M.; Khorasheh, F.; Zarkesh, J., Investigating the effect of calcination repetitions on the lifetime of Co/γ-Al_2O_3 catalysts in Fischer-Tropsch synthesis utilising the precursor's solution affinities. *J. Taiwan Inst. Chem. Eng.,* **2013**. *44*, 205-213, DOI: 10.1016/j.jtice.2012.11.003.

[6] Feyzi, M.; Khodaei, M. M.; Shahmoradi, J., Effect of sulfur on the catalytic performance of Fe–Ni/Al_2O_3 catalysts for light olefins production. *J. Taiwan Inst Chem. Eng,* **2014**. *45*, 452-460, DOI: 10.1016/ j.jtice.2013.05.017.

[7] Dry, M. E., The fischer-tropsch process: 1950-2000. *Catal. Today,* **2002**. *71*, 227-241, DOI: 10.1016/ S0920-5861(01)00453-9.

[8] Dasgupta, D.; Wiltowski, T., Enhancing gas phase Fischer-Tropsch synthesis catalyst design. *Fuel,* **2011**. *90*, 174-181, DOI: 10.1016/j.fuel.2010.07.037.

[9] Hu, J.; Yu, F.; Lu, Y., Application of Fischer-Tropsch synthesis in biomass to liquid conversion. *Catalysts,* **2012**. *2*, 303-326, DOI: 10.3390/catal2020303.

[10] Glasser, D.; Hildebrandt, D.; Liu, X.; Lu, X.; Masuku, C. M., Recent advances in understanding the Fischer-Tropsch synthesis (FTS) reaction. *Curr. Opin. Chem. Eng.,* **2012**. *1*, 296-302, DOI: 10.1016/j.c oche.2012.02.001.

[11] Xu, J.; Bartholomew, C. H., Temperature-programmed hydrogenation (TPH) and in situ Mössbauer spectroscopy studies of carbonaceous species on silica-supported iron Fischer-Tropsch

catalysts. *J. Phys. Chem. B,* **2005**. *109*, 2392-2403, DOI: 10.1021/jp048808j.

[12] Xu, J.; Bartholomew, C. H.; Sudweeks, J.; Eggett, D. L., Design, synthesis, and catalytic properties of silica-supported, Pt-promoted iron Fischer-Tropsch catalysts. *Top. Catal.,* **2003**. *26*, 55-71, DOI: 10.1023/B:TOCA.0000012987.76556.63.

[13] Li, S.; Li, A.; Krishnamoorthy, S.; Iglesia, E., Effects of Zn, Cu and K promoters on the structure and on the reduction, carburization, and catalytic behavior of iron-based Fischer-Tropsch synthesis catalysts. *Catal. Lett.,* **2001**. *77*, 197-205, DOI: 10.1023/A:1013284217689.

[14] Liu, Y.; Teng, B. -T.; Guo, X. -H.; Li, Y.; Chang, J.; Tian, L.; Hao, X.; Wang, Y.; Xiang, H. -W.; Xu, Y.-Y., Effect of reaction conditions on the catalytic performance of Fe-Mn catalyst for Fischer-Tropsch synthesis. *J. Mol. Catal. A: Chem.,* **2007**. *272*, 182-190, DOI: 10.1016/j.molcata.2007.03.046.

[15] Yang, Y.; Xiang, H. -W.; Xu, Y. -Y.; Bai, L.; Li, Y. -W., Effect of potassium promoter on precipitated iron-manganese catalyst for Fischer-Tropsch synthesis. *Appl. Catal., A,* **2004**. *266*, 181-194, DOI: 10.1016/j.apcata.2004.02.018.

[16] Pour, A. N.; Housaindokht, M. R.; Tayyari, S. F.; Zarkesh, J., Kinetics of the water-gas shift reaction in Fischer-Tropsch synthesis over a nano-structured iron catalyst. *J. Nat. Gas Chem.,* **2010**. *19*, 362-368, DOI: 10.1016/S1003-9953(09)60085-2.

[17] Tavasoli, A.; Pour, A. N.; Ahangari, M. G., Kinetics and product distribution studies on ruthenium-promoted cobalt/alumina Fischer-Tropsch synthesis catalyst. *J. Nat. Gas Chem.,* **2010**. *19*, 653-659, DOI: 10.1016/S1003-9953(09)60133-X.

[18] Satterfield, C. N., Heterogeneous catalysis in industrial practice. 2nd Edition, United States: New York, NY (United States); McGraw Hill Book Co., 1991. Print, p. 46-49.

[19] Pour, A. N.; Housaindokht, M. R.; Tayyari, S. F.; Zarkesh, J., Fischer-Tropsch synthesis by nano-structured iron catalyst. *J. Nat. Gas Chem.,* **2010**. *19*, 284-292, DOI: 10.1016/S1003-9953(09)60059-1.

[20] Huff Jr, G. A.; Satterfield, C. N., Intrinsic kinetics of the Fischer-Tropsch synthesis on a reduced fused-magnetite catalyst. *Ind. Eng. Chem. Proc. DD,* **1984**. *23*, 696-705, DOI: 10.1021/i200027a012.

[21] Yates, I. C.; Satterfield, C. N., Effect of carbon dioxide on the kinetics of the Fischer-Tropsch synthesis on iron catalysts. *Ind. Eng. Chem. Res.,* **1989**. *28*, 9-12, DOI:PC/80015-T3ON: DE88007922.

[22] Ghaderi, F.; Ghaderi, A. H.; Najafi, B.; Ghaderi, N.; Viscosity prediction by computational method and artificial neural network approach: The case of six refrigerants. *J. Supercrit. Fluids,* **2013**. *81*, 67-78, DOI: 10.1016/j.supflu.2013.04.017.

[23] Calemma, V.; Correra, S.; Perego, C.; Pollesel, P., Pellegrini, L., Hydroconversion of Fischer-Tropsch waxes: Assessment of the operating conditions effect by factorial design experiments. *Catal. Today,* **2005**. *106*, 282-287, DOI: 10.1016/j.cattod.2005.07.185.

[24] Farias, F.; Rabelo Neto, R.; Baldanza, M.; Schmal, M.; Fernandes, F., Effect of K promoter on the structure and catalytic behavior of supported iron-based catalysts in Fischer-Tropsch synthesis. *Braz. J. Chem. Eng.,* **2011**. *28*, 495-504, DOI: 10.1590/S0104-66322011000300015.

[25] Shiva, M.; Atashi, H.; Mirzaei, A. A.; Arsalanfar, M.; Zare, A., Study of syngas conversion to light olefins by statistical models. *Fuel,* **2014**. *123*, 205-210, DOI: 10.1016/j.fuel.2014.01.064.

[26] Pham, H. N.; Nowicki, L.; Xu, J.; Datye, A. K.; Bukur, D. B.; Bartholomew, C., Attrition resistance of supports for iron Fischer-Tropsch catalysts. *Ind. Eng. Chem. Res.,* **2003**. *42*, 4001-4008, DOI: 10.1021/ie020875h.

[27] Critchfield, B. L., Statistical Methods For Kinetic Modeling Of Fischer Tropsch Synthesis On A Supported Iron Catalyst. Brigham Young University, 2006, pp. 19-23.

[28] Pour, A. N.; Housaindokht, M. R.; Zarkesh, J.; Irani, M.; Babakhani, E. G., Kinetics study of CO hydrogenation on a precipitated iron catalyst. *J. Ind. Eng. Chem. Res.,* **2012**. *18*, 597-603, DOI: 10.1016/j.jiec.2011.11.080.

[29] Butt, J. B., Carbide phases on iron-based Fischer-Tropsch synthesis catalysts part I: Characterization studies. *Catal. Lett.,* **1990**. *7*, 61-81, DOI: 10.1007/BF00764492.

[30] Malessa, R.; Baerns, M., Iron/manganese oxide catalysts for Fischer-Tropsch synthesis. 4. Activity and selectivity. *Ind. Eng. Chem. Res.*, **1988**. *27*, 279-283, DOI: 10.1021/ie00074a013.

[31] Shiva, M.; Atashi, H.; Tabrizi, F. F.; Mirzaei, A. A.; Zare, A., The application of hybrid DOE/ANN methodology in lumped kinetic modeling of Fischer-Tropsch reaction. *Fuel Process. Technol.,* **2013**. *106*, 631-640, DOI: 10.1016/j.fuproc.2012.09.056.

[32] Fazlollahi, F.; Sarkari, M.; Gharebaghi, H.; Atashi, H.; Zarei, M.; Mirzaei, A.; Hecker, W., Preparation of Fe-Mn/K/Al_2O_3 Fischer-Tropsch catalyst and its catalytic kinetics for the hydrogenation of carbon monoxide. *Chin. J. Chem. Eng.,* **2013**. *21*, 507-519, DOI: 10.1016/S1004-9541(13)60503-0.

[33] Tao, Z.; Yang, Y.; Zhang, C.; Li, T.; Ding, M.; Xiang, H.; Li, Y., Study of manganese promoter on a precipitated iron-based catalyst for Fischer-Tropsch synthesis. *J. Nat. Gas Chem.,* **2007**. *16*, 278-285, DOI: 10.1016/S1003-9953(07)60060-7.

[34] Herranz, T.; Rojas, S.; Perez-Alonso, F.; Ojeda, M.; Terreros, P.; Fierro, J., Hydrogenation of carbon oxides over promoted Fe-Mn catalysts prepared by the microemulsion methodology. *Appl. Catal.,* A, **2006**. *311*, 66-75, DOI: 10.1016/j.apcata.2006.06.007.

[35] Zhang, C. -H.; Yang, Y., Teng; B. -T., Li; T. -Z., Zheng; H. -Y., Xiang; H. -W., Li; Y. -W., Study of an iron-manganese Fischer–Tropsch synthesis catalyst promoted with copper. *J. Catal.,* **2006**. *237*, 405-415, DOI: 10.1016/j.jcat.2005.11.004.

[36] Gunst, R. F., Response surface methodology: process and product optimization using designed experiments. *American Statistical Association, Technometrics,* **1996**. *38*, 284-286, DOI: 10.1080/00401706.1996.10484509.

[37] Karimi, F.; Rafiee, S., Taheri-Garavand, A., Karimi, M., Optimization of an air drying process for Artemisia absinthium leaves using response surface and artificial neural network models. *J. Taiwan Inst. Chem. Eng.,* **2012**. *43*, 29-39, DOI: 10.1016/j.jtice.2011.04.005.

[38] Aghaeinejad-Meybodi, A.; Ebadi, A.; Shafiei, S.; Khataee, A.; Rostampour, M., Modeling and optimization of antidepressant drug fluoxetine removal in aqueous media by ozone/H_2O_2 process: comparison of central composite design and artificial neural network approaches. *J. Taiwan Inst. Chem. Eng.,* **2015**. *48*, 40-48, DOI: 10.1016/j.jtice.2014.10.022.

[39] Sodeifian, G.; Sajadian, S. A.; Ardestani, N. S., Evaluation of the response surfaa\ce and hybrid artificial neural network-genetic algorithm methodologies to determine extraction yield of Ferulago angulata through supercritical fluid. *J. Taiwan Inst. Chem. Eng.,* **2015**. *6*, 8, DOI: 10.1016/j.jtice.2015.11.003.

[40] Jaafarzadeh, N.; Ahmadi, M.; Amiri, H.; Yassin, M. H.; Martinez, S. S., Predicting Fenton modification of solid waste vegetable oil industry for arsenic removal using artificial neural networks. *J. Taiwan Inst. Chem. Eng.,* **2012**. *43*, 873-878, DOI: 10.1016/j.jtice.2012.05.008.

[41] Yin, J. -Z.; Xu, Q. -Q.; Wei, W.; Wang, A. -Q., Experiments and numerical simulations of supercritical fluid extraction for Hippophae rhamnoides L seed oil based on artificial neural networks. *Ind. Eng. Chem. Res.,* **2005**. *44*, 7420-7427, DOI: 10.1021/ie049196s.